Magnetic heterogeneity in electron doped $La_{1-x}Ca_xMnO_3$ manganites studied by means of electron spin resonance



2005 J. Phys.: Condens. Matter 17 3903

(http://iopscience.iop.org/0953-8984/17/25/017)

INSTITUTE OF PHYSICS PUBLISHING JOURNAL OF PHYSICS: CONDENSED MATTER

J. Phys.: Condens. Matter **17** (2005) 3903–3914 doi:10.1088/0953-8984/17/25/017

# Magnetic heterogeneity in electron doped $La_{1-x}Ca_xMnO_3$ manganites studied by means of electron spin resonance

**V Likodimos**[1] **and M Pissas**[2]

[1] Physics Department, National Technical University, 157 80 Athens, Greece
[2] Institute of Materials Science, NCSR, Demokritos, 153 10 Aghia Paraskevi, Athens, Greece

Received 14 February 2005, in final form 13 May 2005
Published 10 June 2005
Online at stacks.iop.org/JPhysCM/17/3903

**Abstract**

Electron spin resonance (ESR) has been applied to investigate the magnetic heterogeneity in electron doped $La_{1-x}Ca_xMnO_3$ ($0.80 \leqslant x \leqslant 0.95$). A low field ferromagnetic resonance (FMR) mode is observed for lightly doped compounds ($x = 0.90, 0.95$), signifying the formation of ferromagnetic (FM) spin clusters within the antiferromagnetic G-type AFM phase. The anomalous temperature variations of the resonance field, linewidth and FMR intensity, as well as the observation of thermal cycling effects below $T_C$, emphasize the non-trivial dynamics of the FM phase, which is attributed to the temperature dependent size evolution of the underlying spin clusters towards canted AFM and FM domains. For heavier electron doping ($x = 0.80, 0.85$), distinct AFM behaviour is evinced in the vicinity of $T_N$ in the monoclinic C-type AFM phase, characterized by the absence of critical relaxation. Additional weak FMR lines are observed for $x = 0.80$ and 0.85, whereas a narrow superparamagnetic-like signal is detected for $x = 0.95$.

## 1. Introduction

Spurred on by the observation of colossal magnetoresistance (CMR), mixed-valence manganites have been the focus of intensive research, unveiling a rich phase diagram determined by the strong coupling of spin, charge, orbital and lattice degrees of freedom [1], where intrinsic inhomogeneities signifying phase separation tendencies have been amply identified from a wealth of theoretical and experimental results [2–4]. Phase separation involving coexisting clusters of competing phases in the nanometre or even mesoscopic scale has thus emerged as an intrinsic feature of doped manganites, such as the prototype $La_{1-x}Ca_xMnO_3$ system, leading to an inhomogeneous ground state that is crucial for the pronounced response of their physical properties to relatively small perturbations such as external fields, temperature and chemical doping and the explanation of the CMR effect [4].

  

Stoichiometric $CaMnO_3$ is known to be a band insulator adopting the G-type antiferromagnetic structure (G-AFM) with $T_N \sim 110$ K due to the AFM superexchange coupling between localized $t_{2g}$ spins of $Mn^{4+}$ ions [5]. Experimental investigations have shown that low electron doping results in weak ferromagnetism concomitantly with a metal–insulator transition and CMR in several low bandwidth manganites doped with trivalent rare earth ions [6–11]. Relying on the competition between AFM superexchange and the ferromagnetic (FM) double exchange between itinerant and localized spins, introduction of a small concentration of electrons in the empty $e_g$ band was originally proposed for producing the homogeneous canted G-AFM state [12]. However, recent theoretical work consistently predicts instability of the canted phase against phase separation into FM and AFM states [4, 13–17]. In the electron doped regime of $La_{1-x}Ca_xMnO_3$, systematic experiments have provided evidence for phase separation into local FM regions within the AFM host that vary considerably as a function of doping at low electron densities ($0.00 \leqslant x \leqslant 0.20$) [18–21]. Very recently, detailed investigations by means of neutron powder diffraction and elastic neutron scattering showed a non-trivial microscopic phase separation mechanism involving a small fraction of the doped electrons that segregate into nanoscale FM droplets with a liquid-like spatial distribution along with the formation of an inhomogeneous G-AFM + FM spin canted phase for $0.05 < x \leqslant 0.16$ [22, 23]. Further doping ($x = 0.80, 0.85$) leads to the C-type AFM long range ordering (C-AFM) [5] and the concurrent structural transition from orthorhombic ($Pnma$) to monoclinic ($P2_1/m$) symmetry, characterized by the one-dimensional cooperative ordering of $d(3z^2 - r^2)$ orbitals along which FM double exchange, is confined [24]. At intermediate doping levels ($0.05 < x < 0.20$) the coexistence of the competing C-AFM and G-AFM phases has been evinced by means of neutron diffraction [22, 25], like for other electron doped manganites [26].

Unlike in many experimental methods, where the resolution of AFM + FM phase coexistence from a canted antiferromagnet is hardly accessible, the electron spin resonance (ESR) may serve as a sensitive probe of the local magnetization of paramagnetic, FM and AFM regions even in the case of spin canting, relying on the distinct differences of the corresponding resonance mode spectra. In particular, magnetic anisotropy and exchange fields cause excessive shifts of the effective field used in the equation of motion of the local magnetic moment resulting in widely different resonance conditions, that provide a large contrast between ferromagnetic (FMR) ($T < T_C$) and antiferromagnetic (AFMR) ($T < T_N$) resonance spectra [27].

In this work, we have exploited electron spin resonance (ESR) and magnetization measurements to investigate magnetic homogeneity and phase separation tendencies in the electron doped regime of $La_{1-x}Ca_xMnO_3$($0.80 \leqslant x \leqslant 0.95$). The observation of a low field ferromagnetic resonance (FMR) mode evinced for lighter electron doping ($x = 0.90, 0.95$) supports the formation of FM clusters with $T_C \sim T_N$ (G-AFM). However, the non-monotonic temperature variation of the FMR spectra, as well as the presence of thermal hysteresis, indicates the presence of complicated dynamics of the underlying FM phase. In contrast, only weak FM inhomogeneities are traced for more heavily doped compounds ($x = 0.80, 0.85$), where the monoclinic C-AFM phase is dominant and clear AFM behaviour is observed.

## 2. Experimental details

Polycrystalline samples of $La_{1-x}Ca_xMnO_3$ with $x = 0.80, 0.85, 0.90, 0.95$ were prepared under identical conditions using stoichiometric amounts of high purity $La_2O_3$, $CaCO_3$ and $MnO_2$. Thoroughly mixed powders reacted in air at temperatures up 1400 °C for several days with intermediate grinding and were subsequently cooled at a slow rate to room temperature. Neutron powder diffraction measurements showed that at lower Ca concentrations, $x = 0.80$

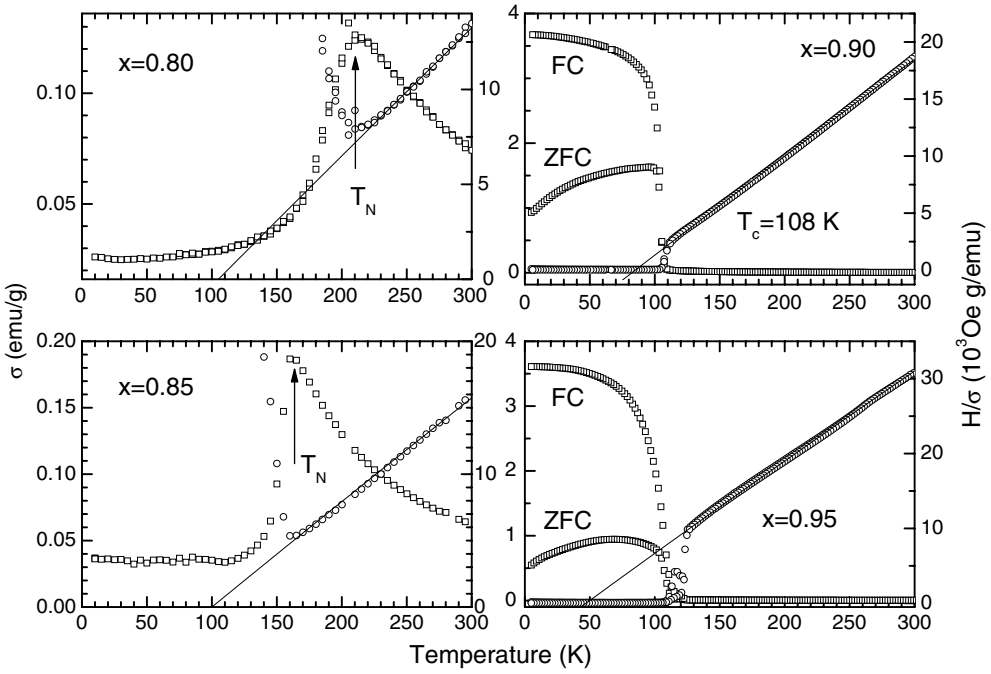


**Figure 1.** Temperature dependence of the magnetic moment per gram (left axes) and inverse mass susceptibility (right axes) for $La_{1-x}Ca_xMnO_3$ ($x = 0.8, 0.85, 0.9$ and 0.95). The straight lines are plots of the equation $\chi^{-1} = (T + \Theta)/(C + (T + \Theta)\chi_o)$.

and 0.85, the samples undergo simultaneously the orthorhombic-to-monoclinic structural transformation and the associated C-AFM ordering at $T_N$ values of 210 and 160 K, respectively [24]. At higher Ca concentrations a mixture of G-AFM and C-AFM phases has been observed along with a ferromagnetic contribution with $T_C \sim T_N$(G-AFM) $\sim$ 110 K [25].

DC magnetization measurements were carried out using a superconducting quantum interference device (SQUID) magnetometer (Quantum Design MPMS2) in the temperature range of 4–300 K, in zero-field cooled (ZFC) and field cooled (FC) modes. ESR measurements were performed with a Bruker ER 200D spectrometer at the X-band ($\nu \approx 9.42$ GHz) using small amounts (4–5 mg) of finely powdered samples either in loose packed form ($x = 0.80, 0.85$) or dispersed in high vacuum grease ($x = 0.90, 0.95$). The magnetic field was scaled with an NMR gaussmeter, while measurements as a function of temperature were carried out in the range of 4–300 K employing an Oxford flow cryostat. Prior to a series of temperature dependent measurements, the sample was rapidly cooled at 4 K and the ESR spectra were subsequently recorded upon heating and then cooling.

## 3. Results

### *3.1. Magnetic measurements*

Figure 1 depicts the temperature variation of the magnetic moment per gram, $\sigma$ (left axes) and $\chi^{-1}$ (right axes) for the samples $x = 0.8, 0.85, 0.9$ and 0.95. According to the neutron diffraction data [24] the sharp drop of the magnetic moment for the samples $x = 0.8$ and 0.85 corresponds to the temperature of transition, $T_N$, from the paramagnetic state to the

C-AFM structure. In the case of samples with $x = 0.9$ and 0.95, although neutron diffraction data are available only for the $x = 0.9$ sample [25], the sharp increase of the magnetic moment corresponds to the onset of a canted magnetic structure. The neutron diffraction data firstly show magnetic Bragg peaks coming from the C-AFM structure and, a few kelvins lower, additional magnetic peaks coming from the G-AFM structure. This coexistence can be attributed to distinct domains with different magnetic structures. The large magnetic moment measured in magnetization measurements, and the significant irreversible behaviour (large difference of the zero-field and field cooled magnetization branches) favour a canted magnetic structure, rather than a mixture of distinct antiferromagnetic domains. We must note that the two antiferromagnetic modes (C and G) become critical at different temperatures.

The inverse susceptibility $\chi^{-1}$ for all samples displays a linear temperature variation above $T_N$ implying Curie–Weiss behaviour, $\chi = C/(T + \Theta) + \chi_o$, where $C = \mu_{eff}^2 \mu_B^2 N_A/(3k_B\,MW)$, $\mu_{eff}^2 = gS(S+1)$, $g$ is the Landé factor, $N_A$ Avogadro's number, $\mu_B$ the Bohr magneton, $k_B$ the Boltzmann constant, $\Theta$ the paramagnetic Curie temperature, MW the molecular weight and $n$ the number of magnetic ions per mole. From the slopes of the experimental $\chi^{-1}$-curves, we estimate $\mu_{eff}$ to be 4.34(1), 3.97(1), 3.73(1) and 3.05(1) for $x = 0.8$, 0.85, 0.9 and 0.95, respectively. The corresponding $\Theta$ values are $-100$, $-105$, $-85$ and $-47$ K. The differences of the paramagnetic Curie temperatures from the corresponding Néel temperatures are related to the fact that the C-type magnetic structure (for $x = 0.8$ and 0.85) and the canted magnetic structure (for $x = 0.9$ and 0.95) are not simple antiferromagnets. In the mean field approximation, the $T_N$ is proportional to the algebraic sum of the nearest-neighbour exchange couplings. The theoretically expected effective magnetic moment $\mu_{eff}^{th}$ for each composition is accordingly given by $\mu_{eff}^{th} = g\sqrt{x S_{Mn^{3+}}(S_{Mn^{3+}}+1) + (1-x)S_{Mn^{4+}}(S_{Mn^{4+}+1)}}$, where $S_{Mn^{3+}} = 3/2$, $S_{Mn^{4+}} = 2$ and $g = 2$ (neglecting spin–orbit coupling). The expected effective magnetic moments are $\sim$4.1, 4.04, 3.98 and 3.93 for $x = 0.8, 0.85, 0.9$ and 0.95, respectively.

### 3.2. *ESR measurements*

*3.2.1. The C-AFM phase ($x = 0.80, 0.85$).* Figure 2 shows representative ESR spectra of the $x = 0.8$ and 0.85 samples as a function of temperature. For $x = 0.80$, a single exchange narrowed resonance line is observed in the paramagnetic regime with $g = 1.985(1)$, due to the strongly coupled $Mn^{4+}$–$Mn^{3+}$ system as in other CMR manganites [28, 29]. The resonance intensity increases slowly as $T_N$(C-AFM) $\approx$ 210 K is approached from above. Below 200 K, the ESR line gradually broadens and its intensity decreases more rapidly, disclosing a rather broad and weak low field resonance, indicative of a small amount of ferromagnetic phase. Lineshape analysis shows that the ESR spectra can be well fitted by the superposition of two separate Lorentzian lines at $T > 150$ K (figure 2 (left panel)), provided that the tail of the resonance absorption at negative field is taken into account, a consequence of the linearly polarized rf field that becomes important when the width becomes comparable to the resonance field. At lower temperatures, the broad ferromagnetic resonance (FMR) can be adequately fitted to a single Lorentz line, which provides an effective description of the FMR lineshape.

Figure 3 summarizes the temperature dependence of the ESR intensity $I_{ESR}$, derived by double integration of the absorption derivative, the resonance field $H_r$ and the linewidth $\Delta H$ (half-width at half-height) of the paramagnetic ESR line for both compounds. For $x = 0.80$, the intensity $I_{ESR}(T)$ shows a broad maximum above $T_N$, similar to the temperature variation of the dc susceptibility, followed by a more rapid decrement down to $T \approx 160$ K, where the ESR line can hardly be discerned. The resonance field $H_r$ does not vary appreciably as

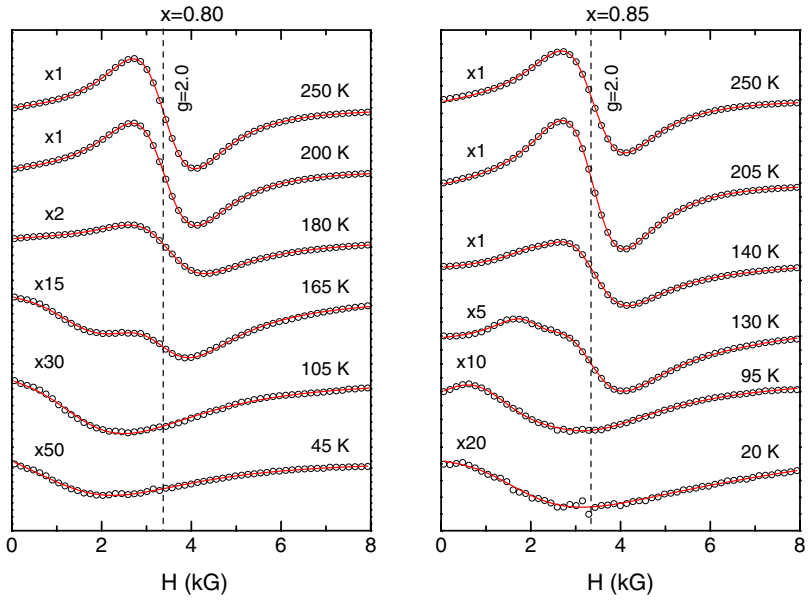


**Figure 2.** Temperature dependence of the ESR spectra (open circles) for $La_{1-x}Ca_xMnO_3$ with $x = 0.8$ (left) and $x = 0.85$ (right) at the X-band ($\nu = 9.415$ GHz). Solid lines correspond to the best-fit lineshape of the total spectrum.

(This figure is in colour only in the electronic version)

$T_N$ is approached from above, while a non-monotonic variation is observed at $T < 200$ K. The ESR linewidth $\Delta H$ exhibits a shallow minimum at $T \approx 220$ K, and then increases considerably at lower temperatures, indicative of inhomogeneous broadening. Suppression of critical relaxation close to $T_N$ (C-AFM) can thus be inferred, in agreement with previous ESR results [28, 30]. However, the finite resonance intensity sustained over a relatively broad temperature range below $T_N$, namely down to $T \approx 160\,\text{K} = 0.76T_N$, is not typical for ordinary AFM transitions, where the energy gap in the antiferromagnetic resonance (AFMR) spectrum attains values much higher than the excitation rf frequency, causing the disappearance of the ESR line in a much narrower temperature range. For example, energy gaps of the spin wave spectra determined by recent AFMR and neutron scattering experiments on hole doped $La_{1-x}A_xMnO_3$ (A = Ca, Sr) have consistently shown values of the order of 600–100 GHz for $0.0 \leqslant x \leqslant 0.1$, where the canted AFM phase has been identified [31–34]. On the other hand, the persistent ESR resonance in the AFM phase and its relatively slow drop correlate well with the gradual growth of the monoclinic distortion, phase fraction and ordered magnetic moment of the C-AFM phase in the same temperature interval for $x = 0.80$ [22, 24].

The broad FMR signal appears from high temperatures for $x = 0.80$, where it is masked by the intense paramagnetic resonance line and causes only a small asymmetry of the lineshape. Considerable variation of both the resonance field and the intensity of the FMR line is derived below $T_N$ (C-AFM) involving initially an increase of both parameters, which subsequently decrease rapidly at $T < 180$ K with their values restored below 160 K, correlating with the suppression of the ESR line and the stabilization of the C-AFM phase. However, this behaviour, indicating that the FMR signal is coupled with the C-AFM transition, relies mostly on the effective decomposition of the two signals by Lorentzian lines, and thus cannot be conclusively determined. Nonetheless, the corresponding resonance intensity $I_{FMR}$ is a rather

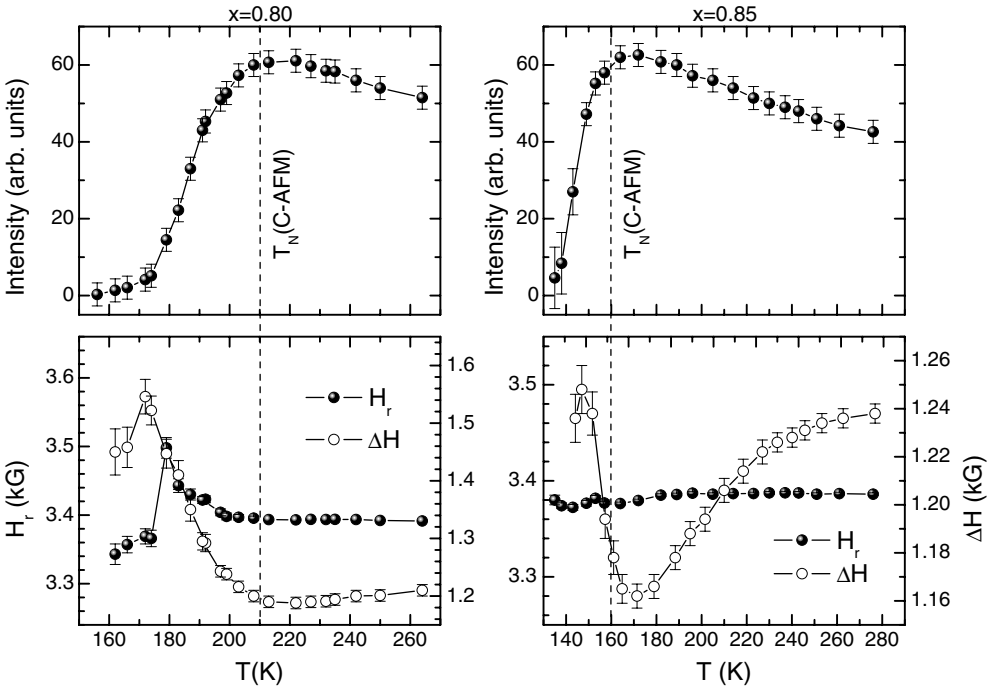


**Figure 3.** Temperature dependence of the ESR intensity (top), resonance field $H_r$ (left axes) and linewidth $\Delta H$ (right axes) of the ESR line for $x = 0.80$ and 0.85. Solid lines connecting the experimental points are guides to the eye. Vertical dashed lines depict the $T_N$ temperatures determined be means of neutron diffraction and dc magnetization.

small fraction of the paramagnetic ESR intensity $I_{ESR}$, approximately 3–4%, hardly detectable in the dc magnetization and neutron diffraction measurements.

For $x = 0.85$, a single ESR line is observed in the paramagnetic regime, which intensifies upon approaching $T_N$(C-AFM) $\approx$ 160 K, and then gradually drops as the temperature decreases to $T \approx 130$ K (figure 2 (right panel)). As the intensity of the paramagnetic ESR line decreases below $T_N$, a weak FMR line appears, more pronounced than for $x = 0.80$, which shifts gradually to lower fields as temperature decreases. Figure 3 (right panel) shows the temperature variation of $I_{ESR}$, $H_r$ and $\Delta H$ of the paramagnetic ESR line. A clear maximum of $I_{ESR}$ is observed at $T \approx 170$ K, which subsequently decreases more rapidly until it disappears over a relatively broad temperature range below $T_N$. The resonance field $H_r$ corresponding to $g = 1.986(1)$ at high temperatures remains practically constant down to 180 K, while the linewidth $\Delta H$ exhibits a small but continuous decrease with a minimum close to $T_N$ and then increases inhomogeneously at lower temperatures. This temperature variation conforms to the gradual build-up of the C-AFM phase and the suppression of critical broadening in the vicinity of $T_N$, as seen for $x = 0.80$. On the other hand, the broad FMR line becomes better resolved and more intense than for $x = 0.80$, indicating an increase of the FM phase content, even though its fraction relative to the high temperature ESR line remains low.

*3.2.2. The C + G-AFM phase ($x = 0.90, 0.95$).* Figure 4 shows the temperature dependence of the ESR spectra for $x = 0.90$, characterized by the coexistence of C-and G-AFM phases and the development of weak ferromagnetism concurrently with the G-AFM transition at

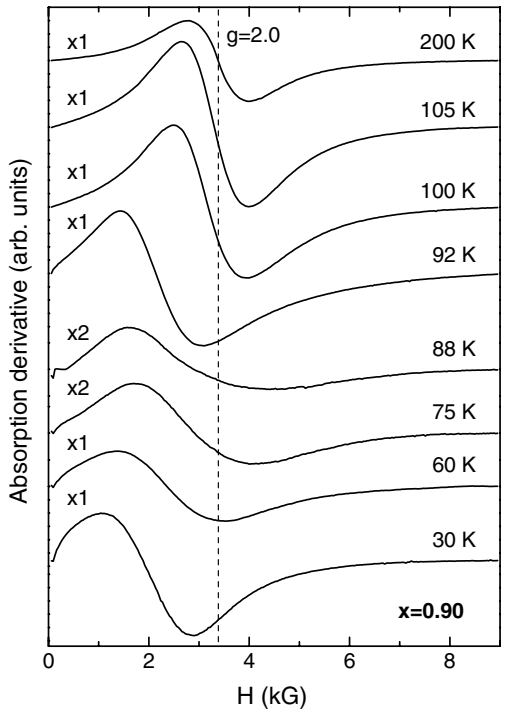


**Figure 4.** Temperature dependence of the ESR spectra for $La_{0.10}Ca_{0.90}MnO_3$ at the X-band ($\nu = 9.414$ GHz).

$T_C \sim T_N$(G-AFM) $\approx 110$ K. In the paramagnetic region, a single ESR line is observed, which shifts rapidly to low fields below 110 K, accompanied by significant lineshape distortion. The temperature variation of the resonance line at $T < T_N$ is not consistent with either of the two resonance modes expected for the homogeneous canted AFM phase, namely the low field FM-like and the high field AFM modes [35], which are commonly observed at much higher frequencies than the X-band [32, 33]. On the contrary, this behaviour is characteristic of the uniform ferromagnetic resonance (FMR) mode appearing below $T_C$ in polycrystalline ferromagnets, where the resonance lineshape is determined by the angular distribution of the local anisotropy axes of the individual crystallites with respect to the applied magnetic field [36–38].

Figure 5 shows the temperature dependence of the apparent resonance field $H_r$ derived from the intersection of the absorption derivative with the baseline, the peak-to-peak linewidth $\Delta H_{pp}$ and the integrated resonance intensity $I$ upon heating and subsequent cooling from high temperatures for $x = 0.90$. A small shift of $H_r$ to lower magnetic fields is observed at $T < 120$ K, followed by a steep decrease below 110 K. This agrees with the increase of the local anisotropy field below the FM transition emerging concomitantly with the G-AFM structure. In particular, the shift of the resonance field to lower fields agrees well with the presence of negative magnetic anisotropy, which causes an effective decrease of $H_r$ as the anisotropy increases [38]. However, a local minimum of the resonance field is observed at $T \approx 90$ K, below which $H_r(T)$ is rapidly restored, succeeded by a smoother temperature decrement, as seen in figure 5(a). This unusual behaviour becomes more pronounced after thermal cycling above $T_C$ which results in a sharp minimum of $H_r(T)$ at $T \approx 90$ K, suggesting a non-monotonic variation of the effective anisotropy. The resonance line broadens rapidly below $T_C$, reaching a maximum concurrently with the minimum of $H_r(T)$ with no appreciable thermal hysteresis, and narrows continuously at lower temperatures, as depicted in figure 5(b).

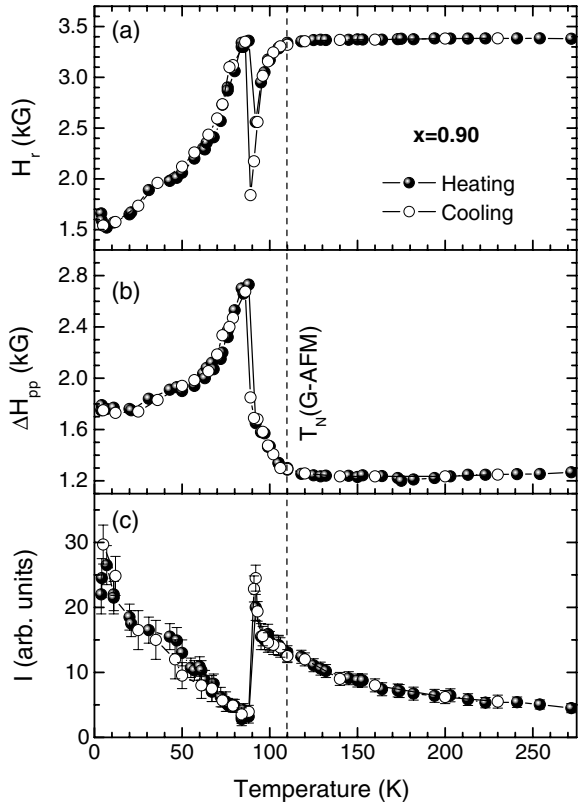


**Figure 5.** Temperature dependence of (a) the resonance field $H_r$, (b) the peak-to-peak linewidth $\Delta H_{pp}$ and (c) the resonance intensity $I$, for $x = 0.90$. Solid lines through the experimental points are guides to the eye.

The broadening of $\Delta H_{pp}$ appears to reflect mainly the anomalous variation of $H_r(T)$ below $T_C$, implying that the FMR linewidth is inhomogeneously broadened by the larger spread of the resonance fields in this temperature range. The resonance intensity $I$ increases continuously down to 90 K, below which an abrupt decrease is detected with negligible thermal hysteresis, followed by an almost linear increase at lower temperatures with a small plateau below 50 K, as shown in figure 5(c).

The irregular loss of FMR intensity is further associated with an increased lineshape asymmetry, which resembles that of metallic samples when the sample thickness becomes comparable to the skin depth, where the skin effect drives electric and magnetic components of the rf field out of phase leading to the admixture of dispersion and absorption spectral components. However, using the specific resistivity $\rho = 10\,\mathrm{m\Omega\,cm}$ reported for polycrystalline $La_{1-x}Ca_xMnO_3$ samples with $x \sim 0.90$ at 100 K [10, 18], we obtain skin depths $\delta(9.4\,\mathrm{GHz}) = 52\ \mu\mathrm{m}$ much larger than the average grain size of the powder specimen (1–3 $\mu$m). This indicates that the persistent lineshape distortion is not determined by the reduced microwave penetration imposed by the skin effect, unless the underlying spin system is due to local regions appreciably more conductive than the bulk. On the other hand, the spectral asymmetry most prominent at 88 K in figure 4 is similar to the FMR powder patterns with negative magnetic anisotropy of cubic or uniaxial symmetry, where $\Delta H_{pp}$ is determined by the distribution of the resonance fields amounting approximately to 5/3 and 3/2 of the magnetic anisotropy field, respectively [36–38].

For $x = 0.95$, an additional narrow ESR line is detected in the paramagnetic region, superimposed on the broader resonance line, which is similar to that observed for $x = 0.90$,

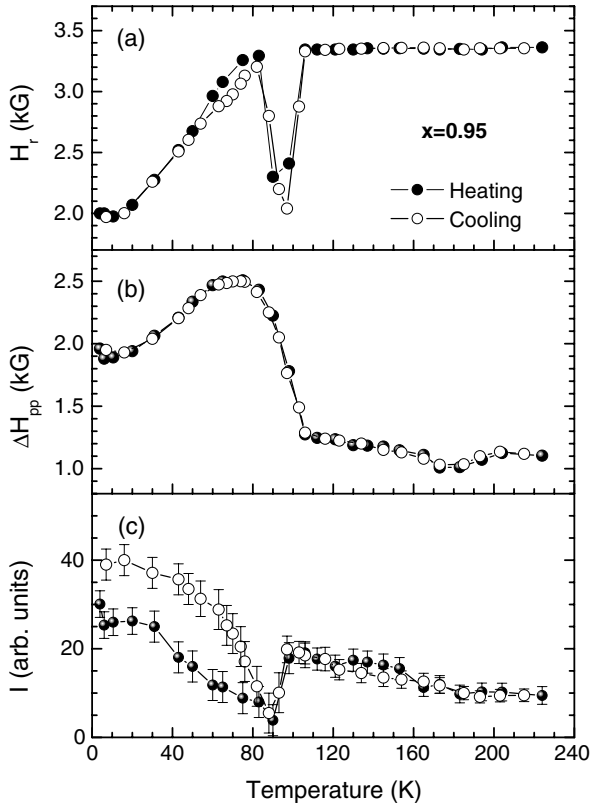


**Figure 6.** Temperature dependence of (a) the resonance field $H_r$, (b) the peak-to-peak linewidth $\Delta H_{pp}$ and (c) the resonance intensity $I$, for $x = 0.95$. Solid lines through the experimental points are guides to the eye.

along with a weak low field absorption signal. At high temperatures ($T > 200$ K), the ESR spectrum can be described by the superposition of two Lorentzian lines with similar $g$-factors, namely a broad and more intense one with $g_1 = 1.986(2)$, $\Delta H_1 = 990(10)$ G and a narrow and weaker one with $g_2 = 1.996(3)$, $\Delta H_2 = 210(15)$ G at 225 K. The intensity of the broad ESR component is about two orders of magnitude larger than that of the narrow one at 225 K, while both lines intensify at lower temperatures. However, additional distortion is observed on the low field side of the ESR spectra at $T < 180$ K, indicating the shift and broadening of the initially narrow ESR component as temperature decreases to 100 K, below which a temperature dependent FMR line similar to that for $x = 0.90$ is detected.

Figure 6 summarizes the temperature dependence of the resonance field $H_r$, peak-to-peak linewidth $\Delta H_{pp}$ and integrated intensity $I$ upon heating and subsequent cooling from high temperatures, reflecting mainly that of the intense ESR component for $x = 0.95$. Compared to the variation of $H_r(T)$ for $x = 0.90$, a steeper decrease of the resonance field is derived below 105 K, followed by a local minimum at $T \approx 95$ K, as shown in figure 6(a). A rapid increase of $\Delta H_{pp}$ is simultaneously observed at $T < 105$ K, reaching a broad maximum that extends to low temperatures, as seen in figure 6(b). The resonance intensity reveals a sharp minimum at $T \approx 95$ K, accompanied by significant thermal hysteresis over the whole temperature range (see figure 6(c)). Further, an anomaly in $\Delta H_{pp}$ is observed at high temperatures ($T \approx 180$ K), closely related to the temperature dependence of the narrow ESR component. Relying on the decomposition of the two ESR components into two independent Lorentz lines at $T > 110$ K, the narrow line is found to shift to lower fields and broaden smoothly from higher temperatures down to 170 K, below which both the resonance field and linewidth vary more rapidly. This

irregularity occurs at the temperature where long range order of C-AFM mesoscopic regions coexisting with the dominant orthorhombic phase is expected [22, 25].

## 4. Discussion

The observation of the low field FMR mode with a similar temperature dependence for the lightly doped compounds ($x = 0.90, 0.95$) allows identifying the formation of FM clusters over a relatively narrow temperature range below $T_N$ (G-AFM), in contrast to the homogeneous canted G-AFM phase. For both samples, the marked drop of the FMR intensity and the simultaneous rise of the FMR linewidth and lineshape asymmetry occur precisely below the distinct dip of $H_r(T)$, pointing to a close relation of these effects. Thermal hysteresis of the magnetization, resistivity and volume expansion has been observed for the electron doped $Sm_{0.15}Ca_{0.85}MnO_3$ manganite, explained by the subtle interplay of G-AFM, C-AFM and FM metastable phases, whose relative volume can be modified by an external magnetic field [39–41]. Recent theoretical work has emphasized the importance of correlated occupation of the FM metallic droplets in analogy to the curvature-driven growth mechanism that reduces the surface tension in domain kinetics as well as the cooperative effects stemming from the long range character of elastic distortions, both leading to the preferential formation of larger clusters, whose size distribution will depend on the thermal history [42, 43].

A rearrangement of the FM droplet distribution might be accordingly proposed to account for the anomalous variation the FMR spectra below $T_N$ (G-AFM), where the average lattice parameters relax [25] and the C- and G-AFM phase fractions become stable [22]. Specifically, an increase of the average size of the FM droplets due to domain growth might be implicated, which would lead to the shift and broadening of the FMR line through the enhancement of the effective magnetic anisotropy. A large increase of the anisotropy field would be, however, required to shift a substantial portion of the FMR resonance intensity out of the scanned field range. On the other hand, a more radical separation into FM clusters with low and high magnetic anisotropy may be conjectured, in accordance with the inhomogeneous magnetism involving cluster formation as well as spin canted regions of finite size within mesoscopic G-AFM domains revealed by neutron scattering [23]. The evolution of a relatively large fraction of FM droplets to regions with high anisotropy such as spin canted G-AFM domains could then lead to the shift of spectral weight to high fields and the reduction of the apparent FMR intensity. This agrees with the relatively large dc magnetization obtained for $x = 0.90$ and 0.95, which is incompatible with the mere presence of the antiferromagnetic G- and C-type structures. The domain nucleation and kinetics would further depend on the crossing of the phase transition from low or high temperatures, leading to the observed thermal hysteresis, which becomes more pronounced upon higher dilution of the FM phase for $x = 0.95$.

Furthermore, the composite, two-line ESR spectra observed at high temperatures for $x = 0.95$ resemble those recently reported for oxygen deficient $LaMnO_{3-\delta}$ and diamagnetically diluted $LaGa_{1-x}Mn_xO_3$ manganites [44]. In these compounds, the narrow ESR component was attributed to spin clusters with weak orbital order that allows for the thermally activated reorientation of the Jahn–Teller configurations and the narrowing of the ESR line at high temperatures. Such an interpretation would agree with the linewidth variation of the narrow ESR line for $x = 0.95$. On the other hand, similar ESR spectra have been observed for dilute suspensions of ferromagnetic nanoparticles in various host matrices [45–48]. In that case, a narrow ESR line at high temperatures is considered as the characteristic feature of superparamagnetic resonance, where thermal fluctuations average out the orientation distribution of the local anisotropy fields, which becomes important at lower temperatures leading to lineshapes similar to the FMR ones for polycrystalline materials [37, 38]. In

particular, the broadening and shift of the superparamagnetic resonance spectra as temperature decreases have been related to thermofluctuational effects on the magnetic anisotropy, while the broad peak in the ESR intensity has been associated with the blocking of the nanoparticle moments [48]. In the present case, the low field shift and broadening of the narrow resonance line, derived from the decomposition of the ESR spectra in the paramagnetic regime, agree favourably with the former effects, indicating FM inhomogeneities. The presence of isolated FM nanoclusters, apart from the FM phase pertaining below $T_N$ (G-AFM), may be accordingly inferred from high temperatures for $x = 0.95$, which is near the phase boundary between G-AFM + isolated FM clusters and the coupled G-AFM + FM cluster glass states [22, 23].

Moreover, the evolution of the weak and broad FMR lines for $x = 0.80$ and 0.85 implies that a small fraction of relatively isolated FM domains may coexist with the dominant C-AFM phase, characterized by one-dimensional FM double exchange. Their formation might be rationalized by local structural inhomogeneities of the monoclinic C-AFM phase promoting FM domain fragments. In this respect, it is possible that the weak ferromagnetism occurring in electron doped $La_{1-x}Ca_xMnO_3$ may involve two different kinds of FM clustered states, one related to the instability of the homogeneous canted G-AFM phase producing the relatively intense low field FMR mode for $x = 0.90, 0.95$, and one associated with inhomogeneities of the monoclinic C-AFM phase, which result in the weak FMR lines for $x = 0.80, 0.85$.

## 5. Conclusions

In conclusion, ESR measurements on electron doped $La_{1-x}Ca_xMnO_3$ reveal a uniform FMR mode supporting the formation of FM spin clusters with $T_C \sim T_N$ (G-AFM) for lightly doped ($x = 0.90, 0.95$) compounds, in contrast to the homogeneous canted G-AFM phase. Distinct anomalies are observed in the temperature variation of the resonance field, linewidth and FMR intensity as well as thermal cycling effects below $T_C$, which can be associated with the temperature dependent size distribution of the underlying FM clusters within the G-AFM matrix. Enhanced magnetic inhomogeneity is inferred for $x = 0.95$, where an additional ESR component is observed from high temperatures following a superparamagnetic-like behaviour, similar to the case for FM nanoparticle suspensions. For heavier doping $x = 0.80, 0.85$, clear AFM behaviour is evinced by ESR near $T_N$ (C-AFM), characterized by the absence of critical relaxation and the relatively slow loss of ESR intensity below $T_N$, suggestive of the gradual growth of the monoclinic C-AFM phase, which is the dominant ground state for this doping regime. Residual FM inhomogeneities are traced for both $x = 0.80$ and 0.85 compositions through the observation of broad FMR lines that vary appreciably near the corresponding C-AFM transition temperatures, appearing as precursors to the phase separation regime evolving for lighter doping.

## References

[1] Ramirez A P 1997 *J. Phys.: Condens. Matter* **9** 8171
Rao C N R and Raveau B (ed) 1998 *Colossal Magnetoresistance, Charge Ordering, and Related Properties of Manganese Oxides* (Singapore: World Scientific)
Coey J M D, Viret M and von Molnár S 1999 *Adv. Phys.* **48** 167
Tokura Y and Tomioka Y 1999 *J. Magn. Magn. Mater.* **200** 1
Rao C N R, Arulraj A, Cheetham A K and Raveau B 2000 *J. Phys.: Condens. Matter* **12** R83
Tokura Y (ed) 2000 *Colossal Magnetoresistive Oxides* (London: Gordon and Breach)
[2] Khomskii D 2000 *Physica* B **280** 325
[3] Mathur N and Littlewood P 2001 *Solid State Commun.* **119** 271
[4] Dagotto E, Hotta T and Moreo A 2001 *Phys. Rep.* **344** 1

[5] Wollan E and Koeller W C 1955 *Phys. Rev.* **100** 545
[6] Troyanchuk I O, Samsonenko N V, Szymczak H and Nabialek A 1997 *J. Solid State Chem.* **131** 144
[7] Martin C, Maignan A, Damay F, Hervieu M and Raveau B 1997 *J. Solid State Chem.* **134** 198
[8] Maignan A, Martin C, Damay F and Raveau B 1998 *Chem. Mater.* **10** 950
[9] Maignan A, Martin C, Damay F, Raveau B and Hejtmanek J 1998 *Phys. Rev.* B **58** 2758
[10] Martin C, Maignan A, Hervieu M and Raveau B 1999 *Phys. Rev.* B **60** 12191
[11] Blasco J, Ritter C, García J, De Teresa J M, Pérez-Cacho J and Ibarra M R 2000 *Phys. Rev.* B **62** 5609
[12] de Gennes P-G 1960 *Phys. Rev.* **118** 141
[13] Nagaev E L 1998 *Phys. Rev.* B **58** 2415
[14] Kagan M Yu, Khomskii D I and Mostovoy M V 1999 *Eur. Phys. J.* B **12** 217
[15] Ohsawa T and Inoue J 2002 *Phys. Rev.* B **65** 134442
[16] Dunaevsky S M and Deriglazov V V 2003 *Phys. Rev.* B **67** 014409
[17] Maitra T and Taraphder A 2003 *Phys. Rev.* B **68** 174416
[18] Neumeier J J and Cohn J L 2000 *Phys. Rev.* B **61** 14319
[19] Granado E, Moreno N O, Martinho H, Garcia A, Sanjurjo J A, Torriani I, Rettori C, Neumeier J J and Oseroff S B 2001 *Phys. Rev. Lett.* **86** 5385
[20] Cohn J L and Neumeier J J 2002 *Phys. Rev.* B **66** 100404(R)
[21] Cornelius A L, Light B E and Neumeier J J 2003 *Phys. Rev.* B **68** 014403
[22] Ling C D, Granado E, Neumeier J J, Lynn J W and Argyriou D N 2003 *Phys. Rev.* B **68** 134439
[23] Granado E, Ling C D, Neumeier J J, Lynn J W and Argyriou D N 2003 *Phys. Rev.* B **68** 134440
[24] Pissas M, Kallias G, Hofmann M and Többens D M 2002 *Phys. Rev.* B **65** 064413
[25] Pissas M and Kallias G 2003 *Phys. Rev.* B **68** 134414
[26] Martin C, Maignan A, Hervieu M, Raveau B, Jirák Z, Savosta M M, Kurbakov A, Trounov V, André G and Bourée F 2000 *Phys. Rev.* B **62** 6442
[27] Morrish A H 1965 *The Physical Principles of Magnetism* (New York: Wiley)
[28] Causa M T, Tovar M, Caneiro A, Prado F, Ibanez G, Ramos C A, Butera A, Alascio B, Obradors X, Pinol S, Rivadulla F, Vázquez-Vázquez C, López-Quintela M A, Rivas J, Tokura Y and Oseroff S B 1998 *Phys. Rev.* B **58** 3233
[29] Ivanshin V A, Deisenhofer J, Krug von Nidda H-A, Loidl A, Mukhin A A, Balbashov A M and Eremin M V 2000 *Phys. Rev.* B **61** 6213
[30] Atsarkin V A, Demidov V V, Simon F, Gaal R, Moritomo Y, Conder K, Jánossy A and Forró L 2003 *J. Magn. Magn. Mater.* **258/259** 256
[31] Biotteau G, Hennion M, Moussa F, Rodríguez-Carvajal J, Pinsard L, Revcolevschi A, Mukovskii Y M and Shulyatev D A 2001 *Phys. Rev.* B **64** 104421
[32] Pimenov A, Biberacher M, Ivannikov D, Loidl A, Ivanov V Yu, Mukhin A A and Balbashov A M 2000 *Phys. Rev.* B **62** 5685
[33] Ivannikov D, Biberacher M, Krug von Nidda H-A, Pimenov A, Loidl A, Mukhin A A and Balbashov A M 2002 *Phys. Rev.* B **65** 214422
[34] Mihály L, Talbayev D, Kiss L F, Zhou J, Fehér T and Jánossy A 2004 *Phys. Rev.* B **69** 024414
[35] Cinader G 1967 *Phys. Rev.* **155** 453
[36] Schlömann E and Zeender J R 1958 *J. Appl. Phys.* **29** 341
[37] Raikher Yu L and Stepanov V I 1992 *Sov. Phys.—JETP* **75** 764
[38] de Biasi E, Ramos C A and Zysler R D 2003 *J. Magn. Magn. Mater.* **262** 235
[39] Mahendiran R, Maignan A, Martin C, Hervieu M and Raveau B 2000 *Phys. Rev.* B **62** 11644
[40] Respaud M, Broto J M, Rakoto H, Vanacken J, Wagner P, Martin C, Maignan A and Raveau B 2001 *Phys. Rev.* B **63** 144426
[41] Algarabel P A, De Teresa J M, García-Landa B, Morellon L, Ibarra M R, Ritter C, Mahendiran R, Maignan A, Hervieu M, Martin C, Raveau B, Kurbakov A and Trounov V 2002 *Phys. Rev.* B **65** 104437
[42] Khomskii D and Khomskii L 2003 *Phys. Rev.* B **67** 052406
[43] Burgy J, Moreo A and Dagotto E 2004 *Phys. Rev. Lett.* **92** 097202
[44] Noginova N, Bah R, Bitok D, Atsarkin V A, Demidov V V and Gudenko S V 2005 *J. Phys.: Condens. Matter* **17** 1259
[45] Sharma V K and Waldner F 1977 *J. Appl. Phys.* **48** 4298
[46] Gazeau F, Shilov V, Bacri J C, Dubois E, Gendron F, Perzynski R, Raikher Yu L and Stepanov V I 1999 *J. Magn. Magn. Mater.* **202** 535
[47] Kliava J and Berger R 1999 *J. Magn. Magn. Mater.* **205** 328
[48] Berger R, Bissey J-C, Kliava J, Daubric H and Estournes C 2001 *J. Magn. Magn. Mater.* **234** 535